

Impact of the amount of the gold layer on the tribological performance of the ceramic conversion treated CP-Titanium

Zhang, Zhenxue; Yu, Hao; Li, Xiaoying; Dong, Hanshan

DOI:

[10.1007/s11249-023-01711-w](https://doi.org/10.1007/s11249-023-01711-w)

License:

Creative Commons: Attribution (CC BY)

Document Version

Publisher's PDF, also known as Version of record

Citation for published version (Harvard):

Zhang, Z, Yu, H, Li, X & Dong, H 2023, 'Impact of the amount of the gold layer on the tribological performance of the ceramic conversion treated CP-Titanium', *Tribology Letters*, vol. 71, no. 2, 36.

<https://doi.org/10.1007/s11249-023-01711-w>

[Link to publication on Research at Birmingham portal](#)

General rights

Unless a licence is specified above, all rights (including copyright and moral rights) in this document are retained by the authors and/or the copyright holders. The express permission of the copyright holder must be obtained for any use of this material other than for purposes permitted by law.

- Users may freely distribute the URL that is used to identify this publication.
- Users may download and/or print one copy of the publication from the University of Birmingham research portal for the purpose of private study or non-commercial research.
- User may use extracts from the document in line with the concept of 'fair dealing' under the Copyright, Designs and Patents Act 1988 (?)
- Users may not further distribute the material nor use it for the purposes of commercial gain.

Where a licence is displayed above, please note the terms and conditions of the licence govern your use of this document.

When citing, please reference the published version.

Take down policy

While the University of Birmingham exercises care and attention in making items available there are rare occasions when an item has been uploaded in error or has been deemed to be commercially or otherwise sensitive.

If you believe that this is the case for this document, please contact UBIRA@lists.bham.ac.uk providing details and we will remove access to the work immediately and investigate.



Impact of the Amount of the Gold Layer on the Tribological Performance of the Ceramic Conversion Treated CP-Titanium

Zhenxue Zhang¹ · Hao Yu¹ · Xiaoying Li¹ · Hanshan Dong¹

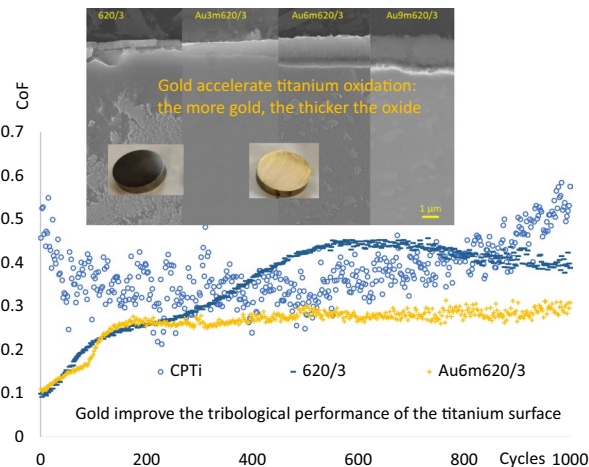
Received: 30 November 2022 / Accepted: 14 February 2023
© The Author(s) 2023

Abstract

Titanium alloys are characterised by poor tribological properties, and a ceramic TiO₂ layer formed on the surface can greatly improve its performance. By pre-depositing a gold layer on the titanium surface, the gold particles promoted the outward diffusion of titanium in the ceramic conversion treatment to react with the inward-coming oxygen to form a compact titanium dioxide layer. The surface morphology, microstructure, and phase constituents were characterised by SEM/EDX and XRD. The adhesion of the oxide layers was assessed by a scratch test. The distribution of gold particles in the oxide layer enhanced the surface hardness and reduced the friction and wear against a WC (tungsten carbide) ball in the reciprocal tribological test. The ceramic conversion process was accelerated efficiently at 620–660 °C, and the more gold pre-deposited, the thicker the oxide layer.

Graphical Abstract

Impact of the amount of the gold layer on the tribological performance of the ceramic conversion treated CP-Titanium



Keywords Gold · Ceramic conversion treatment · Oxidation · CP-Ti · Friction · Wear

1 Introduction

Due to its high strength-to-weight ratio, high biocompatibility and excellent chemical stability, commercially pure titanium (CP-Ti) is used in a wide range of industries such as the fixation of fractures and joint replacements [1]. However,

✉ Zhenxue Zhang
z.zhang.1@bham.ac.uk; zhzhxue@yahoo.com

¹ School of Metallurgy and Materials, The University of Birmingham, Birmingham B15 2TT, UK

titanium has a high and unstable coefficient of friction, strong adhesive tendency and high wear rate [2], thus making it difficult for high-stress and long-term applications like long-spanned fixed prostheses and the frameworks of removable partial dentures [3, 4]. Different surface engineering methods like PVD (physical vapour deposition) [5], CVD (chemical vapour deposition) [6], plasma treatment [7], nitriding [8] and anodization [9] have been used to modify titanium alloys. Among them, ceramic conversion treatment (CCT) can generate a ceramic hard layer supported by a hardened diffusion zone on the surface of the titanium alloys which can greatly improve the tribological performance of titanium alloys [10, 11]. However, the lengthy thermal-chemical process of CCT (50 to 100 h at temperatures ranging from 580 to 700 °C) can result in grain growth of the matrix which negatively affects its mechanical properties [3, 10, 12]. In previous research, we found that gold promoted the outward diffusion of titanium at elevated temperatures and therefore accelerated the oxidation process of CP-Ti and Ti6Al4V alloys [13–15]. Gold is also one of the most promising solid lubricants due to its long-term stability and frictional properties [16]. Furthermore, gold nanoparticles in the TiO₂ film can enhance its photocatalytic [17, 18] and antimicrobial activity [19], etc. There is no previous study on the effect of amount of gold layer on the wear resistance of the ceramic conversion treated CP-Titanium. Therefore, this study aimed to investigate the impact of the thickness of a pre-deposited gold layer on the CCT of CP-Ti to clarify the role of gold in the interaction with pure titanium in oxidation. In the meantime, a variety of performance tests were used to evaluate the hardness, scratch resistance and friction

and wear of the surface to study whether the addition of gold could improve the mechanical performance of CP-Ti, and therefore offer an efficient surface modification of CP-Ti alloy for biomedical application.

2 Experimental

CP-Ti bar (25.4 mm in diameter) was cut into 4.5 mm thick coupons. The coupons were ground progressively from 120 to 1200 grit and then were cleaned in an acetone bath using an ultrasonic cleaner. After drying, gold layers of three thicknesses were pre-deposited on the cleaned CP-Ti coupons. The deposition was carried out at room temperature in an Emscope SC 500 sputter deposition instrument under 25 mA for 3 min (Au3m), 6 min (Au6m) and 9 min (Au9m). Calculated based on the weight gain after deposition, the thicknesses were about 15, 30 and 45 nm separately for Au3m, Au6m and Au8m deposition. CCT was operated in an Elite Thermal Systems Limited electric furnace with a heating rate of 8 °C/min. After treatment, it was cooled down to room temperature in the furnace. Based on our previous research [13, 20], three treatment durations (3, 40 and 80 h) at 620 °C were executed to compare the impact of the different amounts of gold on the CCT (Table 1). A higher temperature CCT (660 °C/3 h) was also used to further verify the impact of gold on the CCT of CP-Ti. The weight change after the CCT was measured via a high-precision balance OHAUS GALAXY 160D. Weight gain per unit surface area ($\Delta W/A$)

Table 1 Ceramic conversion treatment detail of CP-Ti samples with different amount of pre-deposited gold layer

Sample code	Pre-deposition time (minute)	Temperature (°C)	Time (hour)	$\Delta W/A$ ($\mu\text{g}/\text{mm}^2$)	Roughness (R_a , μm)
Untreated	–	–	–	–	0.16 ± 0.02
620/3	–	620	3	1.38	0.22 ± 0.02
Au3m620/3	3			1.97	0.26 ± 0.03
Au6m620/3	6			3.16	0.19 ± 0.03
Au9m620/3	9			3.35	0.17 ± 0.02
620/40	–		40	3.94	0.12 ± 0.02
Au3m620/40	3			5.52	0.16 ± 0.03
Au6m620/40	6			6.51	0.28 ± 0.03
Au9m620/40	9			8.09	0.17 ± 0.03
620/80	–		80	6.71	0.14 ± 0.02
Au3m620/80	3			7.50	0.11 ± 0.02
Au6m620/80	6			8.88	0.25 ± 0.02
Au9m620/80	9			9.66	0.19 ± 0.03
660/3	–	660	3	1.78	0.16 ± 0.02
Au3m660/3	3			3.16	0.20 ± 0.03
Au6m660/3	6			4.93	0.18 ± 0.03
Au9m660/3	9			6.11	0.13 ± 0.03

was calculated to monitor the initial impact of gold on CCT (Table 1).

The roughness (the arithmetic average roughness) of the surface was measured by an XP-200 Plus Stylus Profilometer (Table 1). Surface phase constituents were examined by a powder diffractometer Inel EQUINOX 3000 (2C) X-ray diffraction (XRD) using Cu-K α radiation ($\lambda = 0.154056$ nm). It scanned from 20.01 and up to 80° with a step size of 0.02° and counting times of 2 s/step. CCTed coupons were sectioned and mounted in conductive Bakelite, ground and polished to a mirror-like finish to measure the cross-sectional hardness change. The microstructure was revealed after etching by Kroll's reagent of 2% HF, 10% HNO₃, and 88% H₂O. Surface morphology, cross-sectional microstructure, and elemental information were investigated by a Jeol 7000 scanning electron microscope (SEM) equipped with an Oxford Inca energy dispersive X-ray spectroscopy (EDX) detector.

A Zwick Roell's Indentec hardness testing machine was used for Vickers surface micro-hardness measurement. The load was 25 gf and the holding time was 10 s. A Micro Materials NanoTest system was used to measure the cross-sectional nano-hardness change under a load of 20 mN with a holding time of 5 s. A ST30 Scratch Tester with a Rockwell spherical cone tip was used to evaluate the adhesion/cohesion strength of the converted ceramic layers. An initial load of 5 N was applied and it was increased linearly (10 mm/min) until 60 N. Friction and wear properties of the CCTed surface were tested against an 8 mm in diameter tungsten carbide (WC) ball in a reciprocating sliding mode utilising a phoenix TE-79 multi-axis tribology machine. The temperature was between 20 and 22 °C and the humidity was about 48–52%. A load of 20 N was used for 1000 cycles. The sliding distance was 5 mm with an average sliding speed of 5 mm/s and a frequency of about 0.5 Hz. The geometrical shapes of the wear tracks were plotted by a profilometer, which was used to measure the depth, width and cross-sectional area of the track, and the average area of five locations was used to calculate the volume of material loss. The debris and wear tracks were further analysed by SEM/EDX to study the tribological mechanism.

3 Results

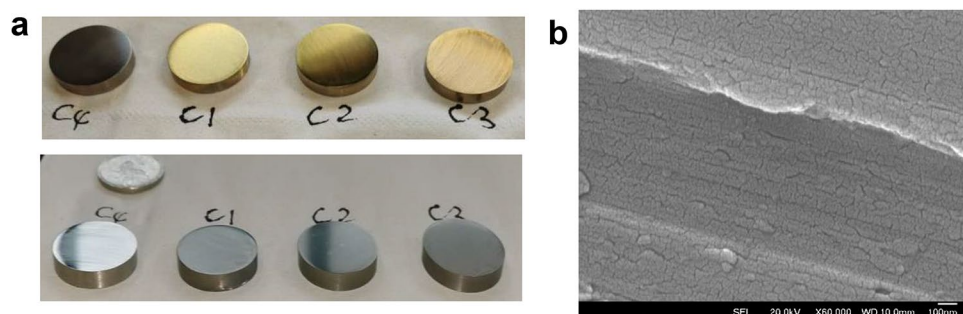
3.1 Surface Morphology and Roughness Change

After the sputter deposition of the gold layer, the sample surface changed from a metallic silver appearance to golden colour, being more obvious with more gold deposited (Fig. 1 top). After CCT, all the samples lost their metallic lustre and turned into different colours indicating the change of surface morphology and roughness. After CCT at 620 °C for 3 h, the surface of CP-Ti showed some light blue colour, while all the gold pre-deposited samples turned into dark grey colour as shown in Fig. 1, and it became darker for samples with more gold pre-deposited. With increasing the treatment time to 40 and 80 h, all the surfaces turned into deep dark grey colour, and so did the samples CCTed at 660 °C for 3 h.

The surface morphology of CP-Ti samples changed considerably after the CCT. For 620 °C/3 h treated samples, there were some white particles evenly dispersed on the surface for gold pre-deposited samples as seen in Fig. 2a–c. Further analyse by EDX under 20 kV (Fig. 3b) indicated that they were gold particles. With the increased amount of pre-deposited gold, the remaining particles on the surface became sparse and smaller (Fig. 2a–c). The grinding marks can still be clearly seen on the surface of sample 620/3 without any gold pre-deposition (Fig. 2d); however, they became less obvious for those samples with gold pre-deposition (Fig. 2a–c). The surface became moderately smoother with more gold pre-deposited (Table 1). Increasing the treatment time at 620 °C to 40 and 80 h, gold particles spread on the surface evenly and grew slightly bigger (Fig. 2e/f), while the roughness value increased slightly in contrast to the sample without gold (Table 1). For a higher temperature CCT (660 °C for 3-h), the same trend with larger gold particles was observed. Interestingly, with more gold pre-deposited on the surface, the gold particles became less populated and smaller for all the treatments for the same condition.

Elemental information on the surface and cross-section was collected and exemplified by the sample Au6m620/80

Fig. 1 **a** Surface appearance change of samples before and after CCT at 620 °C for 3-h: C1-Au9m620/3, C2-Au6m-620/3, C3-Au3m-620/3 and C4-620/3; **b** surface morphology of the gold particles on the surface of C3-Au3m before CCT



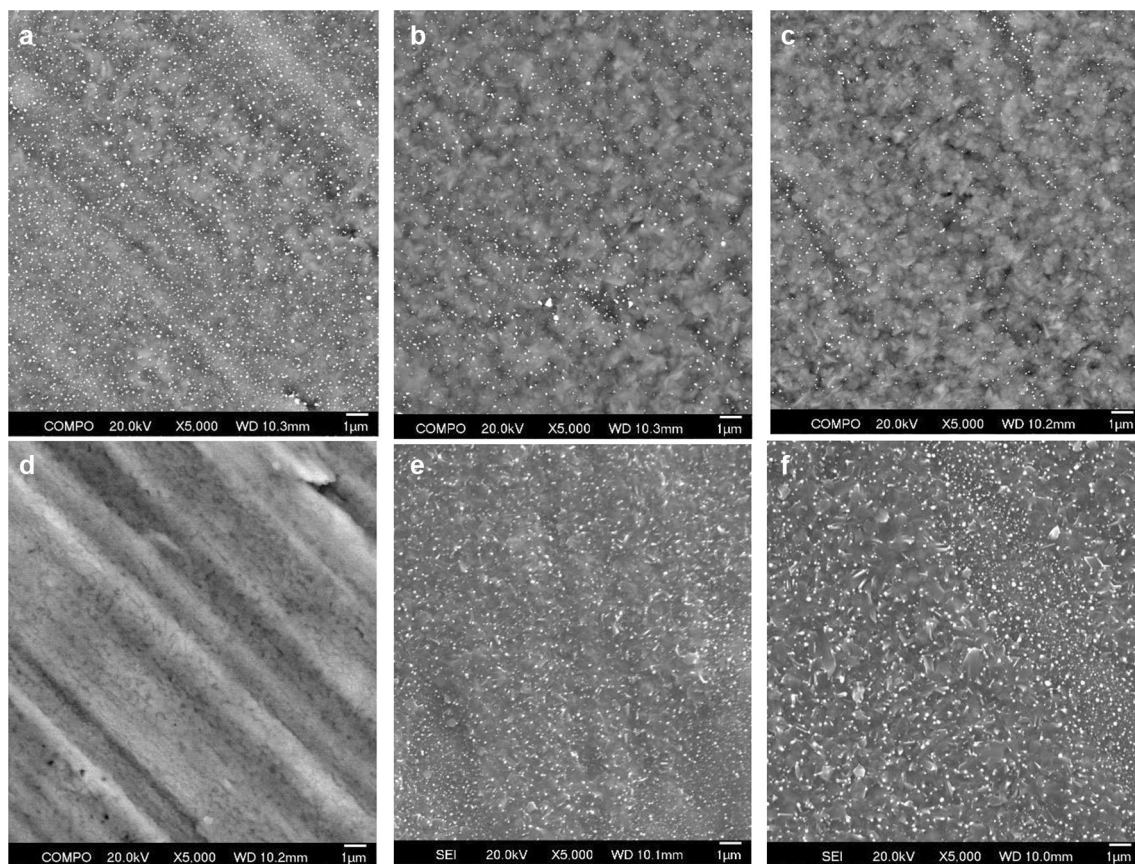


Fig. 2 Surface morphology change of samples after CCT (a) Au_{3m}620/3, (b) Au_{6m}620/3 (c) Au_{9m}620/3, (d) 620/3, (e) Au_{3m}620/40 and (f) Au_{3m}620/80

in Fig. 3. White particles (Spot 1 in Fig. 3b) on the surface were rich in gold, other regions were stoichiometrically TiO₂ (Spot 2 in Fig. 3b) which were similar to the spots 3/4 in Fig. 3d in the oxide layer. The inset picture in Fig. 3a demonstrates the distribution of oxygen, gold and titanium. In a fractured oxide layer (Fig. 3c), the crystalline size in Zone A near the gold line was smaller and denser than in the other zone like B. A smaller amount of gold was detected in the oxide layer through the thickness, and tiny gold particles were evenly dispersed in the oxide layer (Fig. 3d). There was also a clear light colour mark between the oxide layer and matrix and EDX identification suggesting it had a higher content of gold (Spot 5 in Fig. 3d). Oxygen content at spot 6 in Fig. 3d was still higher indicating the oxygen diffused into the matrix during the CCT process.

3.2 Thickness of the Oxide

As shown in Figs. 4 and 5, after 3 h CCT, the thickness of the oxide layers was about 0.2–0.3 µm for CCT without any pre-deposited layer (620/3). However, the thickness of the oxide layer increased significantly with a pre-deposited

gold layer, i.e., 1 µm for sample Au_{3m}620/3. The thickness was also larger with more gold pre-deposited on the surface, 1.5 µm and 1.8 µm for samples Au_{6m}620/3 and Au_{9m}620/3, separately (Fig. 4a). Extending the treatment time to 40 and 80 h, the oxide layer became much thicker for gold pre-deposited samples as evidenced in Figs. 4 and 5. However, for a longer treatment like 80 h, a smaller amount of gold (Au_{3m}620/80) only added a 0.6 µm oxide layer to 2.6 µm from 2 µm (620/80). Double the amount of gold almost doubled the oxide layer thickness, but the difference between 6 min and 9 min pre-deposition was not significant. Apparently, there was a thin gold interfacial layer between the oxide layer and the matrix after CCT. With the increasing amount of the pre-deposited gold, the marker became clearer and thicker as shown in Fig. 4a. With a similar amount of gold pre-deposited on CP-Ti samples, the thickness of the oxide layer increased with treatment time and temperature which generally followed the thermodynamic of oxidation (Fig. 4b).

Fig. 3 EDX analysis on the surface and cross-section of sample Au6m620/80: (a) surface with an inset of local mapping image, (b) selected spots on the surface (c) fractured cross-section (d) selected spots at the oxide layer and matrix, and (e) elemental information

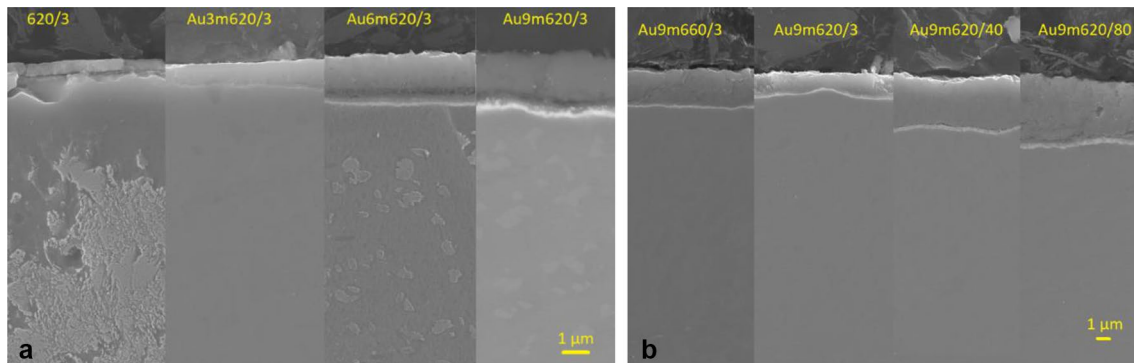
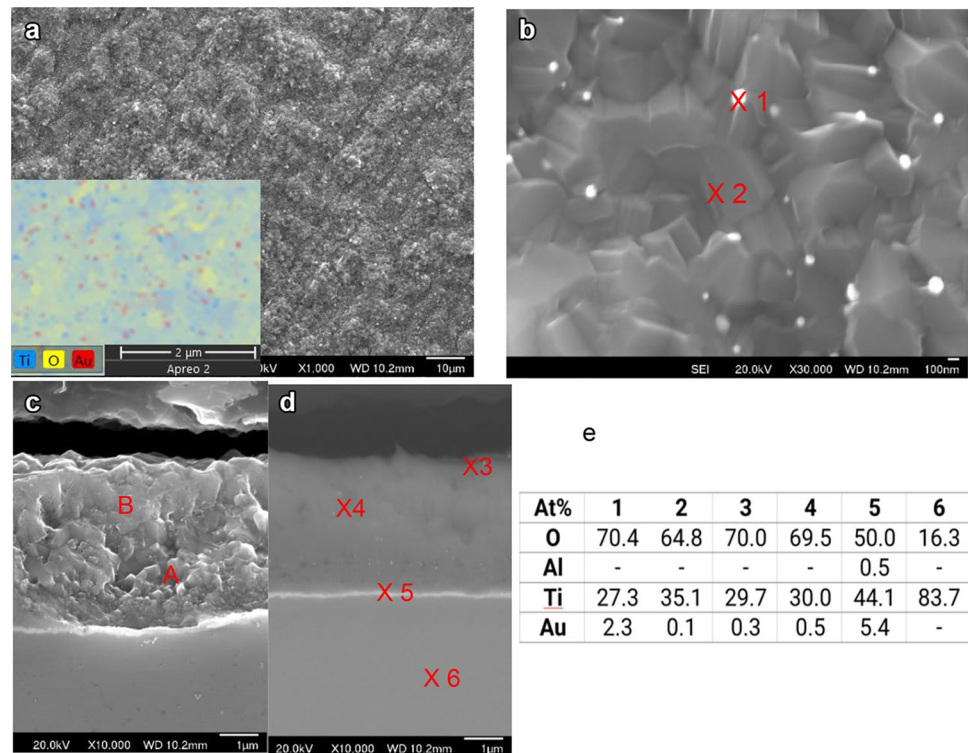


Fig. 4 Cross-sectional view of samples: (a) CCTed at 620 °C for 3 h, (b) 9 min gold-pre-deposited samples after different CCT

3.3 Surface Phase Constituents

The changes in phase constituents on the surface of CPTi samples after CCT are shown in Fig. 6. After 3-h treatment at 620 °C, the three α -Ti peaks (100), (002) and (101) shifted to a lower angle due to the dissolution of the oxygen atom as an interstitial element. Rutile (110) can be identified on the surface of the sample without a pre-deposited gold layer (620/3). With the pre-deposited gold layer, the rutile peaks (110), (101), (200), (111) and (210) became significant and the crystal grew bigger with the increased amount of pre-deposited gold. In the meantime, anatase (101) can also be detected on the surface of the gold pre-deposited sample.

The thickness of the oxide layers increased after a longer treatment time, i.e. 620 °C/80 h, the intensity of the alpha peaks decreased significantly especially on the surface with a higher amount of gold (sample Au9m620/80). Although rutile phases dominated the surface, anatase can still be identified on the surface, a higher amount of gold not only promoted the oxide formation but also benefited the growth of a mixture of anatase and rutile at this temperature range. For the samples CCTed at 620 °C/40 h and 660 °C/3 h, the phase constituents had a similar trend.

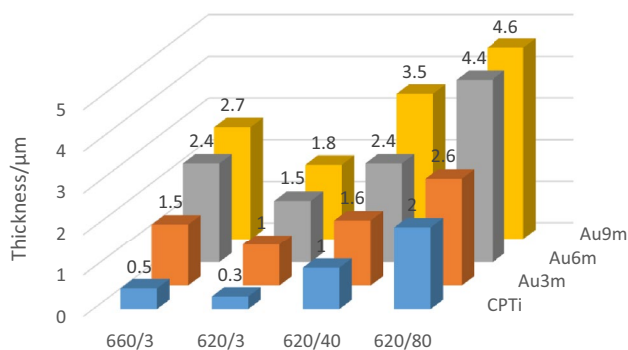


Fig. 5 The oxide thickness change against the treatment temperature and duration for the samples with different amount of gold pre-deposited layer

3.4 Mechanical Properties

3.4.1 Surface Micro-hardness

The surface micro-hardness of the CP-Ti samples increased remarkably after CCT (Fig. 7). After CCT at 620 °C for 3 h, the surface hardness increased from HV_{0.05} 274 (CPTi) to about HV_{0.05} 509 (620/3). All the gold pre-deposited samples had notably higher surface hardness, HV_{0.05} 858, HV_{0.05} 915 and HV_{0.05} 964, for Au3m620/3, Au6m620/3 and Au9m620/3 separately. The higher the amount of gold pre-deposited, the higher the surface hardness after the same CCT. A similar trend of surface hardness change occurred in other CCTs at 620 °C for 40 and 80 h and the treatment at 660 °C for 3 h as shown in Fig. 7.

Fig. 6 Surface phase evolution identified by XRD for CP-Ti samples with different amount of pre-deposited gold. Rutile (JCPDS:86–0147), Anatase (JCPDS:84–1286), α-Ti (JCPDS:44–1294), and Au (JCPDS 04–0784)

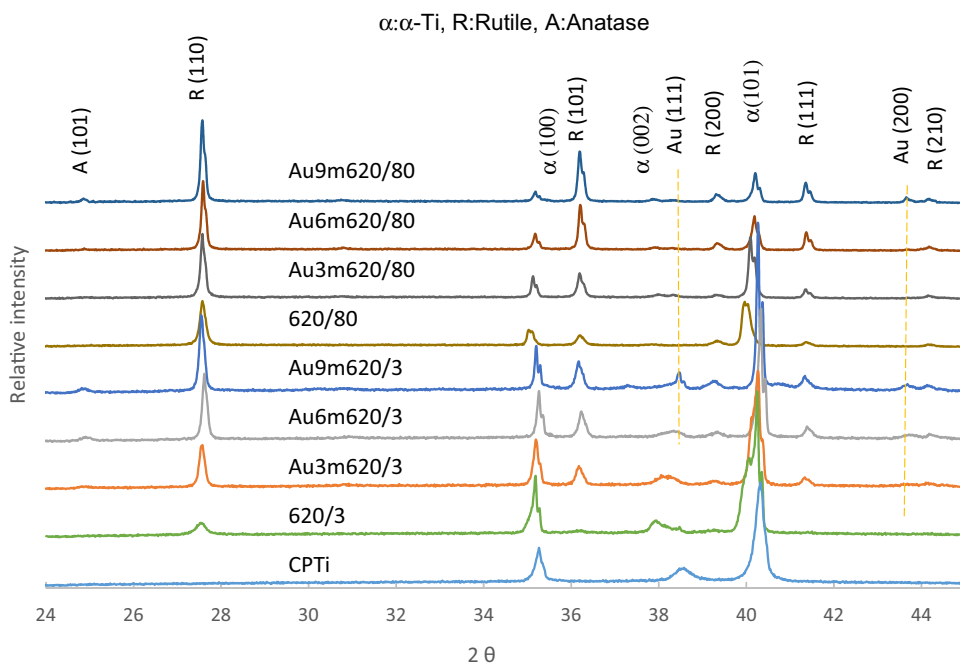


Fig. 7 Vickers surface hardness of CCTed samples

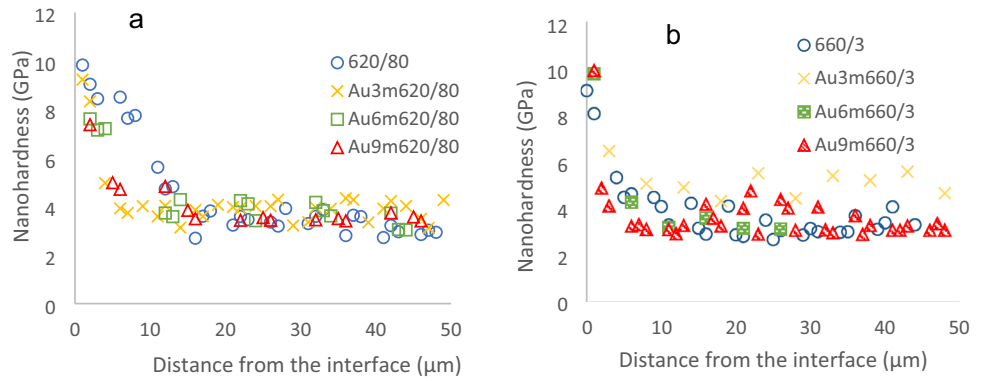
3.4.2 Cross-Sectional Nano-hardness Profiles

Nanoindentation was used to measure the nano-hardness change under the oxide layer, and the cross-sectional nano-hardness depth profiles are plotted in Fig. 8. For CCT treatment at 620 °C for 80 h, there was a clear hardened zone up to 15 μm deep for sample 620/80; however, this zone was reduced to less than 10 μm (Fig. 8a) for those samples pre-deposited with gold. A comparable result was obtained for the sample CCTed at 620 °C for 40 h. A much shallow hardened zone of about 5 μm was found for the 3-h short treatment at 620 and 660 °C as shown in Fig. 8b.

3.4.3 Scratch Testing on the Converted Ceramic Oxide Layers

The scratch tests were carried out on selected samples to examine the adhesion and cohesion of the oxide layers (Fig. 9). For the short time (3-h) treated surfaces, chips appeared at both sides from the beginning of the scratching test. Sample Au3m620/3 failed at about 20 N, and the oxide layer on sample Au9m620/3 was scraped off at an even

Fig. 8 Nano-hardness profile along depth for samples CCTed at (a) 620 °C/80 h and (b) 660 °C/3 h



lower load, indicating more gold in the oxide layer led to a more brittle layer. For the longer treatment, smaller chips started to emerge at the sides for sample 620/80 when the load increased from 5 to 10 N. The number and size of the chips both increased with the increment of the load, and a total failure occurred just under 40 N which was confirmed by the EDX analysis of the path as shown in Fig. 9b, d.

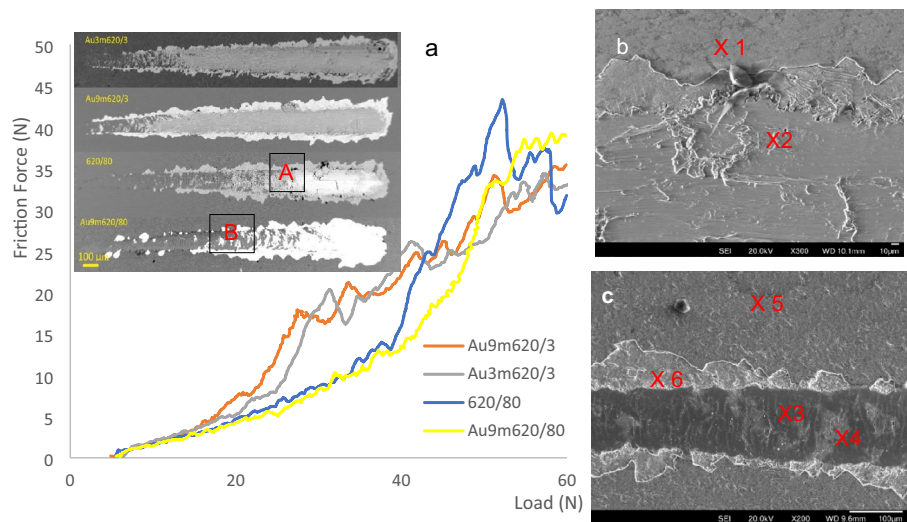
For sample Au9m620/80, larger chips appeared at the sides at a load of 10 N, and the number and size of the chips didn't increase a lot until a load of 30 N (Fig. 9c), part of the oxide layer came off as identified by EDX (Fig. 9d). The chips developed continuously until the end of the test as indicated in Fig. 9a. A total delamination of the oxide layer occurred at a load near 40 N (Fig. 9a) which resembled that of sample 620/80.

3.4.4 Reciprocal Friction and Wear Test Against WC Ball

As demonstrated in Fig. 10a, the coefficient of friction (CoF) of the untreated CP-Ti sample against the WC ball was quite high and unstable. The CoF started high at 0.50 under a load of 20 N and reduced slightly to 0.30–0.40 after a 50 cycles run-in process, it then fluctuated in the range of 0.20–0.40 before climbing again after 800 cycles to about 0.55 at the end of the test. For sample 620/3, the CoF kicked off at 0.1 and rose steadily to about 0.45 after 600 cycles, and then dropped slightly but turned more scattered. For the three samples CCTed at 620 °C/3 h with pre-deposited gold, the initial CoF was about 0.10, and it increased steadily to a level between 0.25 and 0.30 after 50–100 cycles and remained stable till the end of the tribo-test (Fig. 10a).

As displayed in Fig. 10b, the typical wear tracks of all the samples after tribo-test were plotted by a profilometer.

Fig. 9 Scratch test results (a) friction load against normal load curves of 4 samples and BEI images of the scratches (Inset picture), Selected EDX spot analysis on the Zone A (b) and Zone B (c) in the scratch, (d) elemental composition of different points



d

At%	1	2	3	4	5	6
O	72.2	0	66.8	30.5	64.9	25.2
Ti	27.6	99.7	33.1	66.4	35.1	70.6
Au	0	0	0.1	2.8	0	4.2
Al	0.2	0.3	0	0.3	0	0

Fig. 10 Tribotest for samples CCTed at 620°C/3 h (a) Coefficient of friction change against the number of cycles for 1000 cycles at 20 N (a) (b) relevant wear tracks (c) enlarged wear tracks for CCTed samples, inset pictures are SEM images of the track

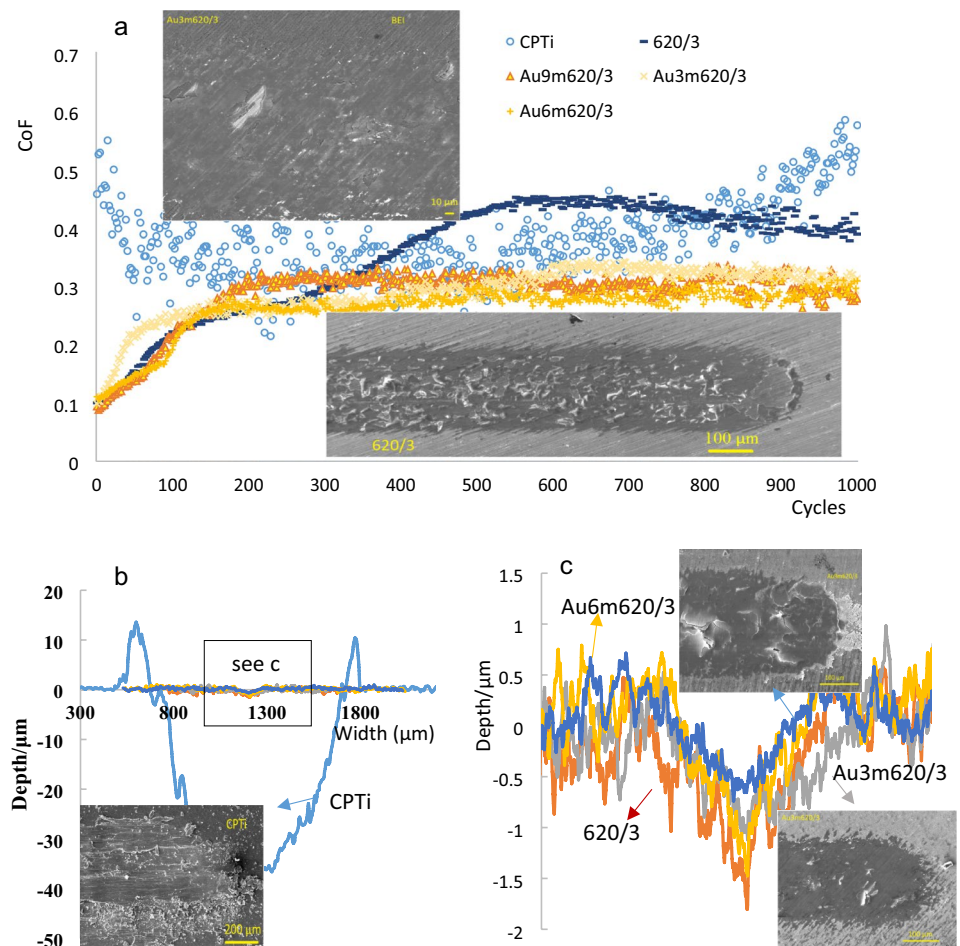


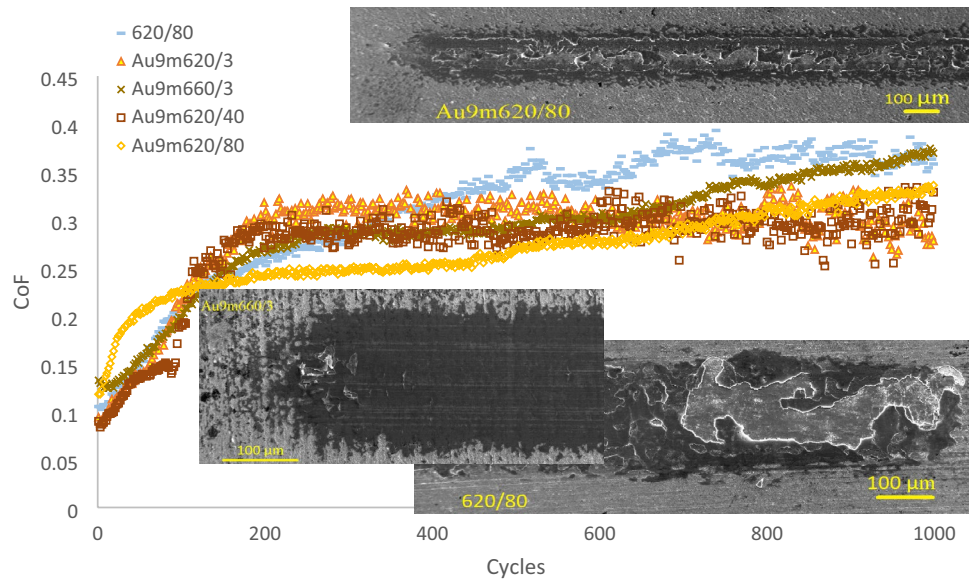
Table 2 Summary of the wear tracks

Sample	Thickness of oxide (μm)	CoF	Wear track width (μm)	Wear track depth (μm)	Wear area (μm^2)	HV _{0.05}	Wear rate (mm^3/Nm)
CPTi	0	0.20–0.58	1087	37	24,450	274 ± 30	1.22E-03
620/3	0.3 ± 0.1	0.10–0.48	243	1.26	147	509 ± 45	7.35E-06
Au3m620/3	1.0 ± 0.2	0.10–0.34	253	1.17	123	858 ± 105	6.15E-06
Au6m620/3	1.5 ± 0.2	0.11–0.31	256	1.06	131	915 ± 112	6.55E-06
Au9m620/3	1.8 ± 0.3	0.09–0.33	189	0.73	71	964 ± 140	3.55E-06
Au9m620/40	3.5 ± 0.3	0.08–0.33	350	2.24	500	1037 ± 106	2.50E-05
Au9m620/80	4.6 ± 0.3	0.12–0.33	204	1.8	156	1505 ± 146	7.80E-06
620/80	2.0 ± 0.2	0.12–0.40	186	0.76	75	1230 ± 150	3.75E-06
Au9m660/3	2.7 ± 0.3	0.13–0.37	236	0.63	61	671 ± 74	3.05E-06

Details about the thickness of the oxide layer, the width/depth of the track, the range of CoF, the wear area, and the calculated wear rate are summarised in Table 2. A deep track of 37 μm with a width of 1087 μm was produced on the untreated CP-Ti sample. The untreated sample had the highest wear rate among all the tested samples and a scuffed

rough wear track with deep plastically deformed grooves and ridges was produced after the tribotest (inset picture in Fig. 10b). A lot of debris was visible in the track which led to high and unstable friction. For sample 620/3 (Inset picture in Fig. 10a), a fractured oxide layer was found in the whole track and some regions were delaminated. A few warped oxide layer pieces can be seen in the track of sample

Fig. 11 Coefficient of friction change against the number of cycles for 1000 cycles at 20 N for samples CCTed at 620°C/80 h and inset pictures of the relevant wear tracks



Au3m620/3 with a much smaller number, furthermore, no total delamination of the oxide layer was found (Fig. 10a). A similar distorted oxide layer was observed in the track of samples Au6m620/3 and Au9m620/3 (Inset pictures in Fig. 10c). With an increased amount of gold in the layer, the wear track was shallower and with a slower wear rate as detailed in Table 2.

As shown in Fig. 11, for the sample CCTed at 620 °C for 80 h, without gold in the oxide layer, the CoF commenced at 0.12 and escalated steadily to about 0.35 after 400 cycles and then oscillated between 0.35 and 0.40, some of the oxide layers were peeled off from the surface as seen in the inset picture in Fig. 11, which might be the reason for the large fluctuations of the CoF in the second half of the tribotest. For the gold pre-deposited Au9m620/80, the onset CoF was about 0.12, it climbed to about 0.25 in the first 100 cycles and then built up smoothly to about 0.33 in the end. Some blisters were found on the worn track and part of the oxide layers were scuffed but it was not exfoliated. The wear rate of Au9m620/80 was higher than that of 620/80. For the sample Au9m620/40, although the CoF had lower inception, it grew rapidly to about 0.30 after 200 cycles and oscillated in the range of 0.25 and 0.35 in the remaining test. Sample Au9m660/3 had an initial CoF of 0.13, and it rose quickly in the first 200 cycles and then climbed gradually to 0.33, however, the wear track was much smoother with a very low wear rate of $3.05 \times 10^{-6} \text{ mm}^3/\text{Nm}$.

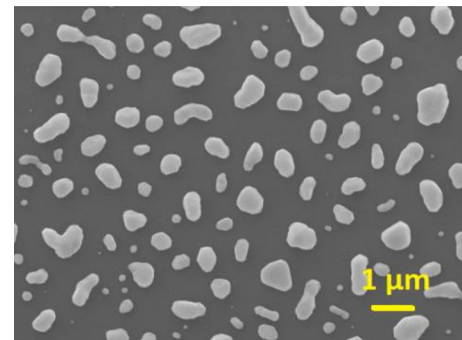


Fig. 12 Gold deposited on silicon wafer (Au6m) after treatment at 620° for 8 h

4 Discussion

In this research, we found that gold can promote the oxidation of titanium, by increasing the amount of pre-deposited gold, this effect demonstrated more significantly. At the same time, the introduction of gold into the oxide layer changed the surface phase constituents and improved the mechanical properties, and therefore it is worthwhile to discuss the mechanism of the pre-deposited gold in the CCT of titanium alloys.

Thanks to the high affinity of Ti for O, the oxidation of titanium alloys is controlled by the dissolution of oxygen in the metal and the outward diffusion of titanium [21, 22]. In our previous study, we found that with the existence of a gold layer on the surface of the titanium alloy, the outward diffusion of Ti ions was promoted to provide more fresh titanium atoms to react with oxygen [13]. Gold has an atomic

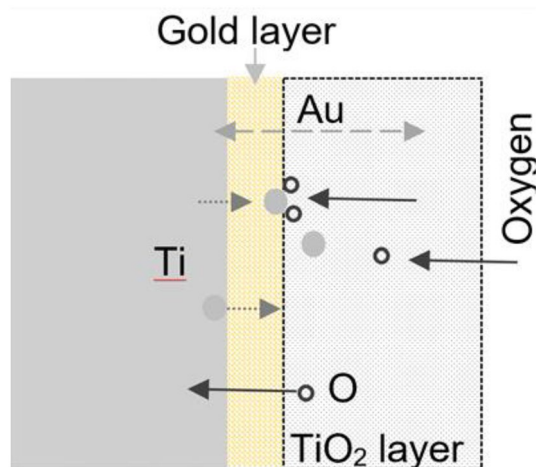


Fig. 13 Mechanism of the oxidation of titanium with gold layer

number of 79 with the electron configuration of $[\text{Xe}] 4f14 5d10 6s1$, and it has a multi-oxidation state. Generally, the nanosized gold particles (Fig. 1b) tended to agglomerate to large zones (Fig. 12) if the gold was not compatible with a substrate like silicon. However, the gold atoms preferentially bound to titanium atoms over oxygen atoms which facilitated the formation of a strongly bonded oxygen/transition-metal system, which can enhance their reactivities [23]. Chen found that gold clusters on oxides had high catalytic activity and gold bilayer structure was significantly more active [24]. O_2 can be adsorbed preferentially at the Au-TiO₂ interface and became ready to dissociate, which acted as a catalyst for the oxidation process [24]. In the initial stages, the presence of gold and its high activity dramatically increased the titanium cations' outward diffusion through the clearance between gold particles (Fig. 1b) to meet the incoming oxygen anions and thus led to the initial increase in the oxidation rate of titanium alloys (Fig. 13). Gold was found at the interface of the oxide layer and within the oxide matrix for all the gold pre-deposited samples.

With more gold-pre-deposited, the oxide layer became thicker under the same treatment conditions (Figs. 4, 5). In the meantime, the gold marker line became wider and spread at the interface zone, especially for the 9 min pre-deposited sample (Fig. 4b). The gold particles had a tendency to diffuse into the matrix of titanium (Fig. 4b) which was in agreement with other researchers' findings [25]. This reciprocal diffusion of gold and titanium made more fresh titanium atoms exposed at the forefront of incoming oxygen atoms/ions to form more oxides. As seen in Fig. 5, with the help of gold, a more linear growth of oxide layer was observed in the test range, however, further evidence is needed to calculate the kinetic rate of the oxidation. During the growth of the oxides, a partial gold marker line was broken, and some smaller particles were left in the path of oxidation

which can be seen on the surface and in the oxide layer. With increasing oxidation time, the lateral diffusion of the gold was responsible for the large gold particles on the surface as evidenced in Fig. 2a, e and f. However, the gold particles on the surface became smaller and sparse for a thick pre-deposited gold layer (Fig. 2a–c) which might be because a thicker oxide layer dispersed the particles more. As reported by Busiakiewicz, a thin gold film formed into gold nanoparticles on rutile titanium dioxide after heat treatment at temperatures of 600 °C [26]. With the increased thickness of the oxide layer, the outward diffusion of the titanium atoms through the oxide layer became difficult, and the inward diffusion of oxygen atoms/ molecules through the oxide layer to react with the titanium at the interface to form the oxide dominated the process, leading to a slower oxidation rate.

As seen in Fig. 6, apart from rutile, some anatase phases appeared on the surface of gold pre-deposited samples which turned clearer with the increasing amount of gold pre-deposited. This was in contrast with another report that rutile was predominately formed on the surface of Ti and its alloys when oxidising at 600–700 °C [20]. However, as rutile TiO₂ is a non-stoichiometric compound represented by TiO_{2-x} and oxygen vacancies are the main defects, doping elements with a higher valence can prevent rutile TiO₂ from forming [27]. Debeila et.al. found that gold particles were mostly on the surface of TiO₂ as metallic gold and no evidence of the substitution of Ti⁴⁺ ions by gold ions in TiO₂, which favoured in the creation of oxygen vacancies and thus promoted the transition of anatase to rutile [28].

Metal and bio-ceramic contact was one of the key considerations of joint replacement, therefore a ceramic WC ball was used as a counterpart ball to test the tribological properties of the titanium alloys samples in a reciprocal mode. A much wider and deeper scuffed track was produced on the untreated CP-Ti sample with the highest wear rate, and the plastically deformed grooves and ridges led to unstable friction (Fig. 10a, b and Table 2). This was probably a result of the formation and periodic localised fracture of a transfer layer [29].

The tough and adherent titanium dioxide layer with enough thickness on the surface of sample 620/80 resulted in a steady CoF and shallow wear track. This was because the oxide layer greatly reduced the adhesive action of metal/ceramic contact (Ti/WC) as a consequence of the nature of the ceramic/ceramic contact (TiO₂/WC) thus reducing the friction and improving the wear resistance of the materials. The CoF became more unsteady after 400 cycles which might be because some of the oxide layers were peeled off (inset picture in Fig. 10b) and the hard ceramic debris led to a more fluctuated friction. However, the wear area and wear rate were much less than that of the untreated CP-Ti (Table 2).

The gold pre-deposited CP-Ti samples all had lower and more stable friction although they increased with the testing time. It was reported that gold in sputtering-produced TiO₂ layer reduced the CoF to 0.16–0.23 against bearing steel in a reciprocating tribotest [30]. Gold particles could self-restore under the applied load because of their low shear strength even if a local failure occurred in the TiO₂ layer, therefore reducing the friction and increasing the wear resistance in a sliding test [31]. However, the track on the samples Au9m620/40 and Au9m620/80 were wider and deeper, and part of the oxide layers was peeled off in the wear track, and this might be due to the oxide layer was too thick (> 3.5 μm). With the increase in thickness, more defects were created in the oxide layer which led to the partial spallation in the scratch and tribotest. For sample Au9m620/3 and sample Au9m660/3, the wear tracks were shallower and smoother, and the wear rate was lower and similar to that of sample 620/80, which could be attributed to a slightly thinner oxide layer (1.8–2.7 μm) with fewer defects. With the assistance of gold, a 3-h treatment can generate an oxide layer with similar tribological performance to that of the 80-h treatment (without any gold pre-deposition), and thus greatly increase the efficiency of ceramic conversion treatment.

5 Conclusions

In this research, a thin gold layer with different thicknesses was used to accelerate the ceramic conversion treatment of commercially pure titanium alloy. A smaller amount (~ 15 nm) of the pre-deposited gold layer accelerated the CCT of the CP-Ti alloy by increasing the thickness of the oxide layer, especially in the initial stages of the treatment (3 h), at temperatures of 620 and 660 °C. With more gold (~ 30 nm) on the surface, the effect became more significant; however, when further increasing the thickness of the gold layer to 45 nm, the oxide layer increased only slightly in comparison to those CCTed at the same condition with less gold.

The gold-rich zone at the interface of the oxide layer and the matrix proved that the gold promoted the outward diffusion of titanium through the gold layer. Gold nanoparticles and clusters were also found in the surface region and the oxide layer after CCT. The surfaces were generally smoother and harder for the samples with a pre-deposited gold layer. They had low and stable friction and very small wear volume thanks to the lubrication of embedded gold nanoparticles and clusters in the compact titanium dioxide layer. However, the gold particles in the oxide layer had a limited effect to improve the adhesion and cohesion of the oxide layer in the scratch test.

With the assistance of pre-deposited gold thin layer, the efficiency of the ceramic conversion treatment increased

significantly. The ceramic oxide layers formed after a 3 h treatment (Au9m620/3, Au9m660/3) achieved similar tribological performance to the typical treatment of 80-h (620/80).

Author contributions Conceptualization, Z.Z. and H.D.; methodology, Z.Z.; investigation, Z.Z. and H.Y.; formal analysis and preparing figures, H.Y., Z.Z. and X.L.; writing—original draft preparation, Z.Z.; writing—review and editing, X.L. and H.D. All authors have read and agreed to the published version of the manuscript.

Funding The authors have not disclosed any funding.

Declarations

Conflict of interest The authors declare that they have no known competing financial interests or personal relationships that could have appeared to influence the work reported in this paper.

Open Access This article is licensed under a Creative Commons Attribution 4.0 International License, which permits use, sharing, adaptation, distribution and reproduction in any medium or format, as long as you give appropriate credit to the original author(s) and the source, provide a link to the Creative Commons licence, and indicate if changes were made. The images or other third party material in this article are included in the article's Creative Commons licence, unless indicated otherwise in a credit line to the material. If material is not included in the article's Creative Commons licence and your intended use is not permitted by statutory regulation or exceeds the permitted use, you will need to obtain permission directly from the copyright holder. To view a copy of this licence, visit <http://creativecommons.org/licenses/by/4.0/>.

References

1. Palka, K., Pokrowiecki, R.: Porous titanium implants: a review. *Adv. Eng. Mater.* **20**, 1700648 (2018). <https://doi.org/10.1002/adem.201700648>
2. Karabakhin, V.G., Zor'kina, N.A.: Antifriction surfacing of titanium alloys. *Weld. Int.* **26**, 409–410 (2012). <https://doi.org/10.1080/09507116.2011.600086>
3. Li, X.; Dong, H. 14 - Ceramic conversion treatment of titanium-based materials. In *Surface Engineering of Light Alloys*, Woodhead Publishing: 2010; 475–500. Doi:<https://doi.org/10.1533/9781845699451.2.475pp>.
4. Jia, D., Zhang, Y., Li, C., Yang, M., Gao, T., Said, Z., Sharma, S.: Lubrication-enhanced mechanisms of titanium alloy grinding using lecithin biolubricant. *Tribol. Int.* **169**, 107461 (2022). <https://doi.org/10.1016/j.triboint.2022.107461>
5. Ben Aissa, C., Khelifi, K.: CAE-PVD synthesis and characterization of titanium-based biocompatible coatings deposited on titanium alloy for biomedical application. *Mater. Today.* **42**, A10–A17 (2021). <https://doi.org/10.1016/j.matpr.2021.04.247>
6. Malhotra, R., Han, Y., Nijhuis, C.A., Silikas, N., Castro Neto, A.H., Rosa, V.: Graphene nanocoating provides superb long-lasting corrosion protection to titanium alloy. *Dent. Mater.* **37**, 1553–1560 (2021). <https://doi.org/10.1016/j.dental.2021.08.004>
7. Rie, K.T., Lampe, T., Eisenberg, S.: plasma heat treatment of titanium and titanium alloy Ti-6Al-4V: effect of gas composition and temperature. *Surf. Eng.* **1**, 198–202 (1985). <https://doi.org/10.1179/sur.1985.1.3.198>

8. Zhu, Y.S., Wei, X.N., Yin, Y.X.: A novel low temperature and green salt bath nitriding of titanium alloy. *Surf. Eng.* **37**, 1422–1431 (2021). <https://doi.org/10.1080/02670844.2021.1979841>
9. Atmani, D., Saoula, N., Abdi, A., Azzaz, M., Wang, Y., Mohamedi, M.: Structural, morphological, and electrochemical corrosion properties of TiO₂ Formed on Ti6Al4V alloys by anodization. *Cryst. Res. Technol.* **53**, 1800138 (2018). <https://doi.org/10.1002/crat.201800138>
10. Dong, H.; Bloyce, A.; Morton, P.M.; Bell, T. Methods of case hardening of titanium alloys. European patent EU: EP1000180, 2001.
11. Çelik, İ, Alsaran, A., Purcek, G.: Effect of different surface oxidation treatments on structural, mechanical and tribological properties of ultrafine-grained titanium. *Surf. Coat. Technol.* **258**, 842–848 (2014). <https://doi.org/10.1016/j.surfcoat.2014.07.073>
12. Guleryuz, H., Cimenoglu, H.: Surface modification of a Ti–6Al–4V alloy by thermal oxidation. *Surf. Coat. Technol.* **192**, 164–170 (2005). <https://doi.org/10.1016/j.surfcoat.2004.05.018>
13. Zhang, Z., Zhang, Y., Li, X., Alexander, J., Dong, H.: An enhanced ceramic conversion treatment of Ti6Al4V alloy surface by a pre-deposited thin gold layer. *J. Alloy. Compd.* **844**, 155867 (2020). <https://doi.org/10.1016/j.jallcom.2020.155867>
14. Zhang, Z.X., Dong, H., Bell, T.: Role of gold in high temperature oxidation of titanium alloy. *Surf. Eng.* **21**, 76–79 (2005)
15. Zhang, Z.X., Dong, H., Bell, T., Xu, B.S.: The effect of gold Pre-deposition on the oxidation behavior of CPTi and Ti6Al4V alloy. *Oxid. Met.* **66**, 91–106 (2006). <https://doi.org/10.1007/s11085-006-9026-x>
16. Antler, M., Spalvins, T.: Lubrication with thin gold films. *Gold Bull.* **21**, 59–68 (1988). <https://doi.org/10.1007/bf03214666>
17. Hussain, M., Ahmad, M., Nisar, A., Sun, H., Karim, S., Khan, M., Khan, S.D., Iqbal, M., Hussain, S.Z.: Enhanced photocatalytic and electrochemical properties of Au nanoparticles supported TiO₂ microspheres. *NJC* **38**, 1424–1432 (2014). <https://doi.org/10.1039/c3nj01525d>
18. Chen, Y., Tang, Y., Luo, S., Liu, C., Li, Y.: TiO₂ nanotube arrays co-loaded with Au nanoparticles and reduced graphene oxide: Facile synthesis and promising photocatalytic application. *J. Alloys Compd.* **578**, 242–248 (2013). <https://doi.org/10.1016/j.jallcom.2013.04.180>
19. Armelao, L., Barreca, D., Bottaro, G., Gasparotto, A., Maccato, C., Maragno, C., Tondello, E., Štangar, U.L., Bergant, M., Mahne, D.: Photocatalytic and antibacterial activity of TiO₂ and Au/TiO₂ nanosystems. *Nanotechnology* **18**, 375709 (2007). <https://doi.org/10.1088/0957-4484/18/37/375709>
20. Dong, H., Bell, T.: Enhanced wear resistance of titanium surfaces by a new thermal oxidation treatment. *Wear* **238**, 131–137 (2000). [https://doi.org/10.1016/S0043-1648\(99\)00359-2](https://doi.org/10.1016/S0043-1648(99)00359-2)
21. Henderson, M.A.: A surface perspective on self-diffusion in rutile TiO₂. *Surf. Sci.* **419**, 174–187 (1999). [https://doi.org/10.1016/S0039-6028\(98\)00778-X](https://doi.org/10.1016/S0039-6028(98)00778-X)
22. Kofstad, P.: High-temperature oxidation of titanium. *J. Less Common Metal.* **12**, 449–464 (1967). [https://doi.org/10.1016/0022-5088\(67\)90017-3](https://doi.org/10.1016/0022-5088(67)90017-3)
23. Hutchings, G.J.: Selective oxidation using supported gold bimetallic and trimetallic nanoparticles. *Catal. Today* **238**, 69–73 (2014). <https://doi.org/10.1016/j.cattod.2014.01.033>
24. Chen, M.S., Goodman, D.W.: The structure of catalytically active gold on titania. *Science* **306**, 252–255 (2004). <https://doi.org/10.1126/science.1102420>
25. Wu, M., Moulin, J., Coste, P., Perrot, S., Perrossier, J.L., Renard, C., Bosseboeuf, A.: Comparative study of Au/Ti, Au/V and Au/Zr films oxygen gettering ability. *Thin Solid Films* **616**, 543–549 (2016). <https://doi.org/10.1016/j.tsf.2016.09.003>
26. Busiakiewicz, A., Kisielewska, A., Piwoński, I., Batory, D., Pabianek, K.: Formation of gold and platinum nanostructures on rutile TiO₂(001) by thermal treatment of thin films in vacuum. *Vacuum* **163**, 248–254 (2019). <https://doi.org/10.1016/j.vacuum.2019.02.026>
27. Yoshihara, M., Miura, K.: Effects of Nb addition on oxidation behavior of TiAl. *Intermetallics* **3**, 357–363 (1995). [https://doi.org/10.1016/0966-9795\(95\)94254-C](https://doi.org/10.1016/0966-9795(95)94254-C)
28. Debeila, M.A., Raphulu, M.C., Mokoena, E., Avalos, M., Petranovskii, V., Coville, N.J., Scurrell, M.S.: The effect of gold on the phase transitions of titania. *Mater. Sci. Eng.* **396**, 61–69 (2005). <https://doi.org/10.1016/j.msea.2004.12.047>
29. Fellah, M., Labaiz, M., Assala, O., Dekhil, L., Taleb, A., Rezag, H., Iost, A.: Tribological behavior of Ti-6Al-4V and Ti-6Al-7Nb Alloys for total hip prosthesis. *Adv. Tribol.* (2014). <https://doi.org/10.1155/2014/451387>
30. Abreu, C.S., Matos, J., Cavaleiro, A., Alves, E., Barradas, N.P., Vaz, F., Torrell, M., Gomes, J.R.: Tribological characterization of TiO₂/Au decorative thin films obtained by PVD magnetron sputtering technology. *Wear* **330**, 419–428 (2015). <https://doi.org/10.1016/j.wear.2015.01.069>
31. Liu, W.-M., Chen, Y.-X., Kou, G.-T., Xu, T., Sun, D.C.: Characterization and mechanical/tribological properties of nano Au–TiO₂ composite thin films prepared by a sol–gel process. *Wear* **254**, 994–1000 (2003). [https://doi.org/10.1016/S0043-1648\(03\)00305-3](https://doi.org/10.1016/S0043-1648(03)00305-3)

Publisher's Note Springer Nature remains neutral with regard to jurisdictional claims in published maps and institutional affiliations.